Global QCD fit from $Q^2=0$ to $Q^2=30\,000$ GeV^2 with Regge-compatible initial condition

G. Soyez

SPhT, CEA Saclay, ORme des Merisiers, Bat 774, F-91191 Gif-sur-Yvette cedex, France

(Received 12 January 2005; published 6 April 2005)

In this paper I show that it is possible to use Regge theory to constrain the initial parton distribution functions of a global Dokshitzer, Gribov, Lipatov, Altarelli, and Parisi (DGLAP) fit. In this approach, both quarks and gluons have the same high-energy behavior which may also be used to describe soft interactions. More precisely, I show that, if we parametrize the parton distributions with a triple-pole pomeron, i.e. like $\log^2(1/x)$ at small x, at $Q^2 = Q_0^2$ and evolve these distributions with the DGLAP equation, we can reproduce F_2^p, F_2^d, F_2^n/F_2^p, $F_2^{\nu N}$, and $xF_3^{\nu N}$ for $W^2 \geq 12.5$ GeV^2. In this case, we obtain a new leading-order global QCD fit with a Regge-compatible initial condition. I shall also show that it is possible to use Regge theory to extend the parton distribution functions to small Q^2. This leads to a description of the structure functions over the whole Q^2 range based on Regge theory at low Q^2 and on QCD at large Q^2. Finally, I shall argue that, at large Q^2, the parton distribution functions obtained from DGLAP evolution and containing an essential singularity at $j = 1$ can be approximated by a triple-pole pomeron behavior.

DOI: 10.1103/PhysRevD.71.076001 PACS numbers: 11.55.–m, 13.60.–r

I. INTRODUCTION

About 30 years ago, Dokshitzer, Gribov, Lipatov, Altarelli, and Parisi (DGLAP) showed [1] that quantum chromodynamics predicts a breakdown of Bjorken scaling in deep inelastic scattering (DIS). Once the parton distribution functions (PDF) are fixed at one initial scale $Q^2 = Q_0^2$, the DGLAP equation gives their evolution to larger values of Q^2. Although the initial equation has only included QCD contributions at leading order (LO) in α_s, the next-to-leading-order (NLO) corrections are now known [2,3] as well as the NNLO corrections [4,5]. There exists a rather large number of global fits (e.g. [6–10]) using the DGLAP equation to reproduce the DIS data. The basic idea is to fix the initial parton distributions, not predicted by perturbative QCD (pQCD), and to evolve it in order to reproduce the experimental measurements as well as possible. The success of this type of analysis is often considered as one of the most important predictions of pQCD.

However, it appears that this approach presents some problems. First, even if the strong rise of F_2 observed by HERA at small x is well reproduced by the DGLAP evolution, this may seem surprising since the evolution generates an unphysical essential singularity which should be replaced by the Balitsky-Fadin-Kuraev-Lipatov (BFKL) small-x behavior [11] which is not observed in the data and is unstable against NLO corrections [12]. Second, the initial parton distributions, at $Q^2 = Q_0^2$, are not predicted by pQCD. We have to parametrize their x dependence and this introduces a large number of free parameters in the models. The resulting distributions often result in a x dependence in contradiction with S-matrix theory [13–15]. To illustrate this, let us consider, for example, the MRST2002 [6] initial conditions: at small x, we have

$$xq(x, Q_0^2) = Ax^{-0.12}, \qquad xg(x, Q_0^2) = Bx^{-0.27} + Cx^{0.00}.$$

These singularities in x do not correspond to any singularity present in hadronic cross sections [16–19] and, conversely, cross-section singularities are not present in parton distributions. There should therefore exist a mechanism explaining how the residues of these singularities in partonic distributions vanish when Q^2 goes to zero, and how the residues of the singularities observed in the total cross sections vanish for nonzero Q^2. Such a mechanism is unknown and seems forbidden in Regge theory, hence a description of both total cross sections and partonic distributions with the same singularity structure seems necessary.

Recent studies [20,21] have shown that it was possible to use Regge theory as an input for DGLAP evolution. In this way, once we have chosen a Regge behavior for the small-x amplitudes, the same x dependence is used for the initial parton distribution and the above-mentioned problem is not present. However, all these works study only the small-x domain. As a consequence, they only take into account the proton structure function and only require one flavor-singlet and one flavor-non-singlet quark distribution in addition to the gluon density. This sometimes requires one to use an external PDF set to describe the large-x domain.

The purpose of the present paper is to use these constraints coming from Regge theory and to show that they apply to global QCD analysis. Practically, we shall assume a Regge behavior, for both quark and gluons, described by a triple-pole pomeron (squared logarithm of x)

$$A\log^2(1/x) + B\log(1/x) + C + D\left(\frac{1}{x}\right)^{-\eta},$$

which is known to give very good descriptions of the soft data. The extension to the large-x region shall be done by introducing powers of $1 - x$ in the initial distributions. In this way, we shall have a description of all structure functions leading to a complete standard PDF set with

 © 2005 The American Physical Society

initial parton distribution having, by construction, a correct analytical behavior in the small-x region.

Since Regge theory is usually used to describe soft amplitudes, we shall also consider the extension of the initial parametrization to low-Q^2 values. Using standard techniques, we shall show that it is possible to continue the initial parton distributions to small Q^2 (Q^2 smaller than the initial scale for DGLAP evolution). In this way, we have a transition between the soft and hard sectors, the former being described by S-matrix theory and the latter being governed by DGLAP evolution. It is worth pointing out that, due to their choice of initial condition, such a description is not possible in usual global fits. This shows that using Regge theory to constrain initial parton distributions in global fits is a very powerful tool.

Finally, we shall show that, at large Q^2, the parton distributions obtained from DGLAP evolution, containing an essential singularity, can be approximated by a squared logarithm of $1/x$ within estimated DGLAP uncertainties. This confirms the results obtained in [22] where we have shown that the residues of the triple-pole pomeron can be extracted from DGLAP evolution.

As mentioned above, some partial results were previously published [18,20,23]. The purpose of the present paper is to turn these fragments into a coherent global description, which can be used as a standard set. Hence, this paper will be as self-contained as possible.

We should also point out that a different approach in trying to reconcile Regge theory with DGLAP evolution has been introduced by Donnachie and Landshoff [24]. However, the present approach is different in the sense that we keep the full DGLAP evolution equation, without taking only the residue at the leading singularity.

II. FITTED AND EVOLVED QUANTITIES

If we want to extend the parametrization introduced in [20] up to $x = 1$, we cannot restrict ourselves only to F_2^p. In order to have a good determination of the valence quarks and of the sea asymmetry, we also need to include other structure functions, measured in the large-x region. In this global fit, we thus include the following quantities:

(i) The proton structure function F_2^p [25–43]: this is by far the most important type of experimental data. Moreover, it is nearly the only one to contribute to the fit in the small-x or in the high-Q^2 region.

(ii) The deuteron structure function F_2^d [41–44]: as we shall see, these data allow the determination of the sea asymmetry. Many points are available in the large- and middle-x regions, where the sea asymmetry is expected to be large.

(iii) The neutrino structure functions $F_2^{\nu N}$ and $F_3^{\nu N}$ [45–47]: these data, in which most of the points are at large values of x, are important to fix the strange quark and the valence-quark distributions. Note that the data considered here are averaged over neutrinos and antineutrinos.

(iv) The F_2^n/F_2^p measurements [48]: these data constrain the valence-quark distributions and the sea asymmetry.

Once we know which experiments are fitted, we must find which quantities need to be evolved. Since the Q^2 range under consideration in global fits extends up to 30 000 GeV^2, we need to consider 5 quark flavors: u, d, s, c, and b. In order to use DGLAP evolution, it is easier to perform linear combinations of the quark distributions. In our case, we shall use 6 flavor-non-singlet distributions

$$\begin{gathered} xu_V = x(u - \bar{u}), \qquad xd_V = x(d - \bar{d}), \\ T_3 = x(u^+ - d^+), \qquad T_8 = x(u^+ + d^+ - 2s^+), \\ T_{15} = x(u^+ + d^+ + s^+ - 3c^+), \\ T_{24} = x(u^+ + d^+ + s^+ + c^+ - 4b^+), \end{gathered} \tag{1}$$

where $q^+ = q + \bar{q}$. Note that since the proton does not contain constituent strange, charm, or bottom valence quarks, we have $s = \bar{s}$, $c = \bar{c}$, and $b = \bar{b}$. At leading order, the Q^2 evolution of each of these distributions is given by the DGLAP equation with the splitting $xP_{qq}(x)$. In addition to the nonsinglet distributions, we have the singlet quark distribution

$$\Sigma = x(u^+ + d^+ + s^+ + c^+ + b^+)$$

which evolves coupled to the gluon distribution $G = xg$, with the full splitting matrix

$$\begin{pmatrix} xP_{qq}(x) & 2n_f xP_{qg}(x) \\ xP_{gq}(x) & xP_{gg}(x) \end{pmatrix}.$$

We shall assume that for $Q^2 \leq 4m_q^2$, the quark q does not enter into the evolution equations.

If we invert the relations (1) and express the quark densities q^+ in terms of the evolved quantities, we obtain

$$\begin{aligned} xu^+ &= \frac{1}{60}(12\Sigma + 3T_{24} + 5T_{15} + 10T_8 + 30T_3), \\ xd^+ &= \frac{1}{60}(12\Sigma + 3T_{24} + 5T_{15} + 10T_8 - 30T_3), \\ xs^+ &= \frac{1}{60}(12\Sigma + 3T_{24} + 5T_{15} - 20T_8), \\ xc^+ &= \frac{1}{20}(4\Sigma + T_{24} - 5T_{15}), \\ xb^+ &= \frac{1}{5}(\Sigma - T_{24}). \end{aligned}$$

Now, we can of course write the structure functions considered here in terms of the parton distributions or in terms of the flavor-singlet and flavor-non-singlet distributions.[1] If, for the sake of clarity, we include other quantities

[1] At leading order, the quark coefficient functions are proportional to $\delta(1 - x)$ and the gluon coefficient function vanishes.

like the neutron structure function, this gives

$$F_2^p = \frac{4x}{9}(u^+ + c^+) + \frac{x}{9}(d^+ + s^+ + b^+) = \frac{1}{90}(22\Sigma + 3T_{24} - 5T_{15} + 5T_8 + 15T_3),$$
$$F_2^n = \frac{4x}{9}(d^+ + c^+) + \frac{x}{9}(u^+ + s^+ + b^+) = \frac{1}{90}(22\Sigma + 3T_{24} - 5T_{15} + 5T_8 - 15T_3),$$
$$F_2^d = \frac{F_2^p + F_2^n}{2} = \frac{5x}{18}(u^+ + d^+) + \frac{4x}{9}c^+ + \frac{x}{9}(s^+ + b^+) = \frac{1}{90}(22\Sigma + 3T_{24} - 5T_{15} + 5T_8),$$

and for the neutrino structure functions

$$F_2^{\nu p} = 2x(d + s + b + \bar{u} + \bar{c}), \qquad F_2^{\nu n} = 2x(u + s + b + \bar{d} + \bar{c}), \qquad F_2^{\bar{\nu} p} = 2x(u + c + \bar{d} + \bar{s} + \bar{b}),$$
$$F_2^{\bar{\nu} n} = 2x(d + c + \bar{u} + \bar{s} + \bar{b}), \qquad xF_3^{\nu p} = 2x(d + s + b - \bar{u} - \bar{c}), \qquad xF_3^{\nu n} = 2x(u + s + b - \bar{d} - \bar{c}),$$
$$xF_3^{\bar{\nu} p} = 2x(u + c - \bar{d} - \bar{s} - \bar{b}), \qquad xF_3^{\bar{\nu} n} = 2x(d + c - \bar{u} - \bar{s} - \bar{b}).$$

If we average over proton and neutron targets, we obtain the neutrino-nucleon structure functions[2]

$$F_2^{\nu N} = F_2^{\bar{\nu} N} = x(u^+ + d^+ + s^+ + c^+ + b^+), \qquad xF_3^{\nu N} = x(u_V + d_V + s^+ - c^+ + b^+),$$
$$xF_3^{\bar{\nu} N} = x(u_V + d_V - s^+ + c^+ - b^+).$$

We may finally average over neutrinos and antineutrinos, which leads to

$$F_2^{(-)^N_\nu} = x(u^+ + d^+ + s^+ + c^+), \qquad = \Sigma,$$
$$xF_3^{(-)^N_\nu} = x(u_V + d_V).$$

III. INITIAL PARAMETRIZATION

If we want to perform a DGLAP evolution, we need to fix the parton distribution functions at an initial scale Q_0^2. Following the same ideas as in [20], we shall parametrize each quark distribution as the sum of a triple-pole pomeron term and an a_2/f-Reggeon term. In addition, each distribution will be multiplied by a power of $(1 - x)$, to ensure that the parametrization extended to $x = 1$ goes to 0 when $x \to 1$. This leads to the following parametrization:

$$xq(x, Q_0^2) = [A_q \log^2(1/x) + B_q \log(1/x) + C_q + D_q x^\eta] \times (1 - x)^{b_q},$$

with[3] $q = u_V, d_V, u_s, d_s, s_s, c_s$, and g. Fortunately, we can restrict many of the 35 parameters introduced here:

(i) First of all, the charm (bottom) distribution will be set to zero for $Q^2 \leq 4m_c^2$ ($Q^2 \leq 4m_b^2$). We shall therefore take $Q_0^2 \leq 4m_c^2$ so that we can set $c(x, Q_0^2) = 0$ and $b(x, Q_0^2) = 0$. In other words, we have $T_{15}(x, Q^2) = \Sigma(x, Q^2)$ for $Q^2 \leq 4m_c^2$ and $T_{24}(x, Q^2) = \Sigma(x, Q^2)$ for $Q^2 \leq 4m_b^2$.

(ii) The pomeron does not distinguish between quarks and antiquarks. This means that the valence distributions u_V and d_V do not contain a pomeron term.

(iii) The pomeron, having vacuum quantum numbers, is insensitive to quark flavor. Thus, the only parameter through which the quark flavor may influence the pomeron is its mass. In other words, the couplings A_q, B_q, and C_q are functions of Q^2 and m_q^2 only. Consequently, the pomeron contributions to the u_s and d_s densities are the same. Assuming that the strange mass is very small compared to the virtualities Q^2 under consideration, we shall also take the same pomeron contribution[4] in s_s.

$$A_u = A_d = A_s = A, \qquad B_u = B_d = B_s = B,$$
$$C_u = C_d = C_s = C.$$

(iv) We shall assume that the Reggeon, being mainly constituted of quarks, does not contribute to the gluon distribution. The parameter D_g will thus[5] be set to 0.

(v) We know from [49] that, at large x, the following behavior is stable with respect to the DGLAP

[2]Neutrino experiments are often performed with heavy nuclei which means that the averaged structure function is measured.

[3]The sea distribution q_s is simply $\frac{1}{2}q^+$.

[4]If we insert an overall factor in s_s, the fit naturally sets it to 1.

[5]If we do not impose $D_g = 0$, the parameter stays small in the fit.

evolution:

$$\Sigma \sim (1-x)^b, \qquad G \sim \frac{(1-x)^{b+1}}{\log(\frac{1}{1-x})}.$$

The denominator $\log(1-x)$ in the gluon distribution does not have a good behavior at small x so we have not included it.[6] Nevertheless, we shall impose

$$b_u = b_d = b_s = b, \qquad b_g = b+1.$$

(vi) If we look at the large-x data, we can see that if we use only $Dx^\eta(1-x)^b$ for the valence quarks, the resulting distribution is too wide, or has a peak at too small a value of x. In order to solve that problem, we have multiplied the valence-quark distributions by a factor $(1+\gamma_q x)$.

(vii) Finally, we still need to impose sum rules. Quark-number conservation can be used to fix the valence-quark normalization factors. If we write

$$A_{u_V} = \frac{2}{N_u} \quad \text{and} \quad A_{d_V} = \frac{1}{N_d},$$

we find

$$N_q = \frac{\Gamma(b_q+1)\Gamma(\eta)}{\Gamma(\eta+b_q+1)}\left(1+\frac{\gamma_q\eta}{\eta+b_q+1}\right). \quad (2)$$

The momentum sum rule is used to fix the constant term C_g in the gluon distribution. Although all the functions involved are analytically integrable, the resulting expression for C_g is quite complicated and we give it in the Appendix.

Taking all these considerations into account, we obtain the following parametrization for the initial distributions:

$$\begin{aligned}
xu_s &= [A\log^2(1/x) + B\log(1/x) + C + D_u x^\eta](1-x)^b, & xu_V &= \tfrac{2}{N_u^*}x^\eta(1+\gamma_u x)(1-x)^{b_u},\\
xd_s &= [A\log^2(1/x) + B\log(1/x) + C + D_d x^\eta](1-x)^b, & xd_V &= \tfrac{1}{N_d^*}x^\eta(1+\gamma_d x)(1-x)^{b_d},\\
xs_s &= [A\log^2(1/x) + B\log(1/x) + C + D_s x^\eta](1-x)^b, & xc_s &= 0,\\
xg &= [A_g\log^2(1/x) + B_g\log(1/x) + C_g^*](1-x)^{b+1}, & xb_s &= 0,
\end{aligned} \quad (3)$$

where the parameters marked with an asterisk are constrained by sum rules.

IV. FITTED EXPERIMENTS

As said previously, we have fitted F_2^p, F_2^d, $F_2^{\nu N}$, $xF_3^{\nu N}$, and F_2^n/F_2^p. We shall now detail which experiments are included in the fit for all these quantities.

For the proton structure function, we have fitted the experiments from[7] H1 [25–31], ZEUS [32–39], BCDMS [40], E665 [41], NMC [42], and SLAC [43]. For the deuteron structure function measurements, we have included data from BCDMS [44] E665 [41], and NMC [42]. We have also taken into account the measurements of F_2^n/F_2^p from NMC [48]. Finally, the neutrino data used here come from CCFR [45–47].

Among all these experimental papers, some give, besides the statistical and the systematic errors, an additional normalization uncertainty. For each of these subsets of the data, we have allowed an overall normalization factor. Let R_i be the normalization uncertainty for the subset i, and ρ_i the effective normalization factor. We may easily minimize the χ^2 with respect to this parameter by requiring

$$\frac{\partial\chi^2}{\partial\rho_i} = \frac{\partial}{\partial\rho_i}\sum_j \frac{(\rho_i d_j - t_j)^2}{\varepsilon_j^2} = 0,$$

where j runs over the data in the subset i. d_j, ε_j, and t_j are, respectively, the jth data, its uncertainty, and the associated theoretical prediction. We easily find

$$\rho_i = \frac{\sum_j \frac{d_j t_j}{\varepsilon_j^2}}{\sum_j \frac{d_j^2}{\varepsilon_j^2}}.$$

Finally, we shall require that ρ_i does not lead to a normalization bigger than the uncertainty R_i. This means that we shall constrain ρ_i to verify

$$1 - R_i \le \rho_i \le 1 + R_i.$$

Before going to the result, one must point out that we have used here the latest CCFR data[8] from 2001 [47].

[6] One solution is to multiply the gluon distribution by an overall factor x. This makes no change at large x and ensures a good behavior at small x because, when $x \to 0$,

$$\frac{x}{\log(\frac{1}{1-x})} \to 1.$$

Numerically, including this factor in the gluon distribution makes only a small correction.

[7] The data set is coming from the DURHAM database (http://durpdg.dur.ac.uk) to which we have added the 2000 and 2001 data from HERA [30,31,39] as well as the reanalyzed CCFR 2001 data [47].

[8] They consist of a reanalysis of the 1997 data.

TABLE I. Values of the fitted parameters in the parton distributions. The last three parameters are not fitted but are obtained from sum rules.

Parameter	Value	Error
A	0.008 76	0.000 43
B	0.019 7	0.0035
C	0.000	0.017
A_g	0.258	0.032
B_g	−0.62	0.25
D_u	0.378	0.030
D_d	0.480	0.030
D_s	0.000	0.013
η	0.392	0.019
γ_u	7.46	0.91
γ_d	9.1	1.6
b_u	3.625	0.016
b_d	5.261	0.086
b	6.67	0.27
N_u	2.015	...
N_d	1.723	...
C_g	3.158	...

These data from Yang's thesis are used by adding the errors in quadrature and, in order to solve a discrepancy with the other data, we have also allowed an overall normalization factor of at most 3%.

V. RESULTS OF THE DGLAP GLOBAL FIT

We have adjusted the 14 parameters A, B, C, A_g, B_g, D_u, D_d, D_s, b, b_u, b_d, γ_u, γ_d, and η to the experimental data in the region

$$Q^2 \geq 4m_c^2 = 6.76 \text{ GeV}^2, \qquad W^2 \geq 12.5 \text{ GeV}^2.$$

The second boundary is used to cut the region where higher-twist effects are expected to be large and we have adopted the same limit on W^2 as MRST. The values of the fitted parameters are presented in Table I and the results, detailed experiment by experiment, are given in Table II. In addition, the curves resulting from our fit are presented for each experiment in Figs. 1–13.

We can see from the parameter table that both the large-x exponents and the Reggeon intercept have acceptable values. One has to notice that quark counting rules predicts the large-x exponents [50] $b_u = b_d = 3$, $b = 5$

TABLE II. Fit results detailed experiment by experiment. For comparison we have added the predictions for CTEQ6 at leading and next-to-leading order (the NLO predictions are taken in the DIS scheme). In the comparison with CTEQ, the results are given with and without taking into account our normalization factors. In this Table and Table IV, ''Quant.'' stands for ''quantity,'' ''nop'' for ''number of points,'' and ''Norm.'' means ''normalized.''

Experiment information						This fit	CTEQ6 LO		CTEQ6 NLO	
Quant.	Collab.	Reference	Nb Pts	ρ_i (%)	χ^2	χ^2/nop	norm.	¬ norm.	norm.	¬ norm.
F_2^p	BCDMS	PLB223(1989)485	167	...	154.607	0.926	5.303	5.303	2.652	2.652
	E665	PRD54(1996)3006	30	1.80	40.368	1.346	1.177	1.233	1.251	1.383
	H1	EPJC19(2001)269	126	−1.50	129.673	1.029	1.516	1.626	1.077	1.122
		EPJC21(2001)33	86	...	75.774	0.881	0.942	0.942	1.008	1.008
		EPJC13(2000)609	130	−1.50	117.682	0.905	1.612	1.962	0.882	1.032
		NPB470(1996)3	156	...	104.206	0.668	0.835	0.835	0.658	0.658
		NPB439(1995)471	90	−4.50	49.499	0.550	0.597	0.901	0.574	0.737
		NPB407(1993)515	21	−8.00	6.233	0.297	0.289	0.466	0.287	0.401
	NMC	NPB483(1997)3	79	2.10	101.927	1.290	1.728	1.260	1.138	1.186
	SLAC	PLB282(1992)475	52	...	97.861	1.882	2.123	2.123	1.355	1.355
	ZEUS	EPJC21(2001)443	214	...	207.294	0.969	2.454	2.454	0.875	0.875
		EPJC7(1999)609	12	...	11.297	0.941	0.744	0.744	1.259	1.259
		ZPC72(1996)399	172	...	238.882	1.389	1.299	1.299	1.429	1.429
		ZPC65(1995)379	56	2.00	27.477	0.491	0.495	0.415	0.453	0.470
		ZPC69(1995)607	9	−1.54	11.493	1.277	1.201	1.270	1.309	1.289
		PLB316(1993)412	17	6.94	6.048	0.356	0.370	0.372	0.344	0.474
	Total		1417		1380.321	0.974	1.864	1.900	1.150	1.187
F_2^d	BCDMS	PLB237(1989)592	154	...	127.941	0.831	1.546	1.546	0.903	0.903
	E665	PRD54(1996)3006	30	...	33.563	1.119	0.913	0.913	1.132	1.132
	NMC	NPB483(1997)3	79	1.00	90.330	1.143	1.438	1.131	0.969	1.071
	SLAC	SLAC-357(1990)	50	...	98.376	1.968	2.515	2.515	1.278	1.278
	Total		313		350.210	1.119	1.613	1.536	1.002	1.027
$F_2^{\nu N}$	CCFR	Yang's thesis	65	3.00	165.512	2.546	3.118	4.570	3.523	6.135
$xF_3^{\nu N}$	CCFR	PRL79(1997)1213	76	...	42.066	0.554	0.658	0.658	1.252	1.252
F_2^n/F_2^p	NMC	NPB371(1995)3	91	...	116.720	1.283	1.315	1.315	1.285	1.285
Total			1962		2054.830	**1.047**	1.794	1.855	1.215	1.333

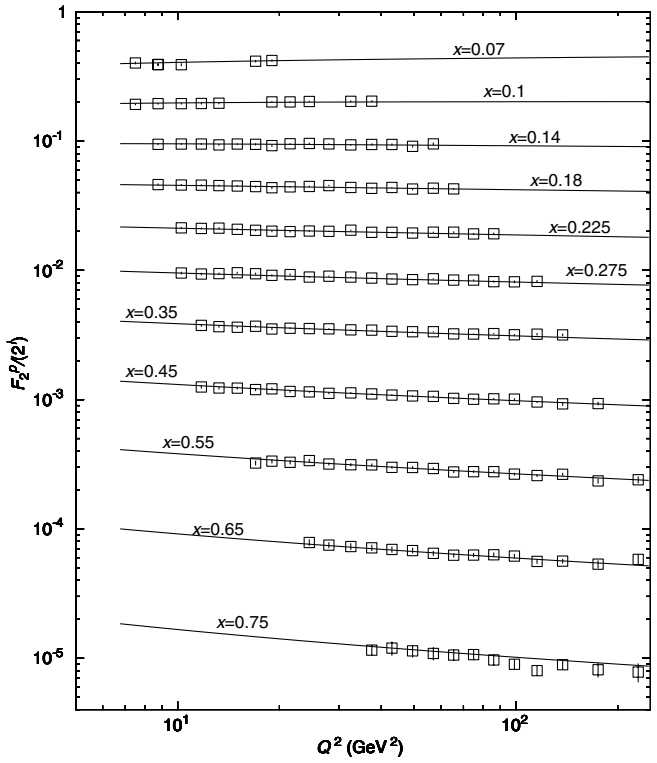

FIG. 1. DGLAP evolution results for BCDMS F_2^p data ($i = 0$ for the upper curve and is increased by 1 from one curve to the next one).

and the same exponent for sea quarks and gluons. However, an analysis of the DGLAP equation at large x [49] shows that these exponents cannot be the same for sea quarks and gluons and are Q^2 dependent. We can still compare our values with those obtained in standard sets. Both CTEQ and MRST find $b_u \sim 3$, $b_d \sim 5$, and $b \sim 7$, hence we obtain parameters of the same order of magnitude.

In order to evaluate the quality of our fit, we have also shown in Table II the CTEQ6 results [8] at LO and at NLO (in the DIS scheme[9]), with and without taking the normalization factors into account.[10] We see that the CCFR 2001 neutrino data probably need to be renormalized up and are still poorly reproduced. We can also see that, apart from the SLAC data, we obtain a very good description. This means that it would be a good idea to add a renormalization factor of a few percent to the SLAC F_2^p and F_2^d data.

The correlation matrix for the parameters is presented in Table III.

[9]The DIS scheme is the renormalization scheme where, at any order, the quark coefficient function is $\delta(1-x)$ and the gluon coefficient function vanishes.

[10]The CTEQ6 results are obtained by using the last CTEQ parton distributions to predict structure functions without any refit. Therefore, the LO and NLO results are just given for comparison.

In Fig. 14, we have shown some typical distributions and their Q^2 evolution. The xu_V and xd_V valence quark distributions both present a peak around $x \approx 0.1$–0.2 and are, roughly speaking, within a factor 2. The sea asymmetry $\bar{d} - \bar{u}$ can be written in the following form:

$$x(\bar{d} - \bar{u}) = \frac{xu_V - xd_V - T_3}{2} = (D_d - D_u)x^\eta(1-x)^b.$$

This distribution has a maximum for

$$x = \frac{\eta}{b+\eta} \approx \begin{cases} 0.1 & \text{for } xu_V, \\ 0.07 & \text{for } xd_V, \\ 0.056 & \text{for } x(\bar{d} - \bar{u}). \end{cases}$$

The evolution in Q^2 of these three distributions shows the same behavior: the peak is moved to smaller values of x and tamed while its width grows. We have also shown in Fig. 14 the gluon distribution which grows quickly with Q^2.

The parton densities at various scales are plotted in Fig. 15. First of all, when $Q^2 = Q_0^2 = 4m_c^2$, we have no charm or bottom quark and both quark and gluon distributions are described by Regge theory, more precisely by a triple-pole and a Reggeon contribution. At higher virtualities, charm quarks are nonvanishing and, for $Q^2 > 4m_b^2$, we also have b quarks. For $Q^2 > Q_0^2$, the parton distributions have an essential singularity at $j = 1$.

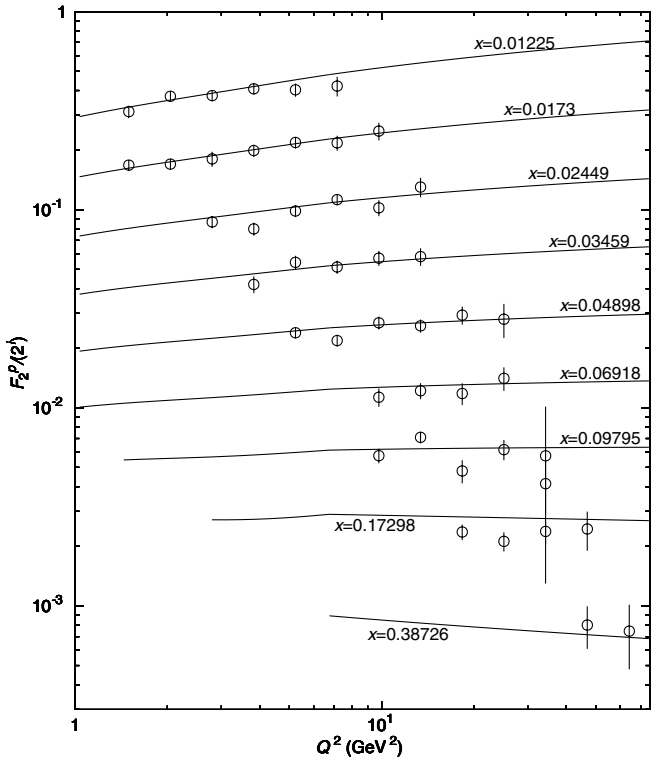

FIG. 2. DGLAP evolution results for E665 F_2^p data. $i = 0$ for the upper curve and is increased by 1 from one curve to the next one.

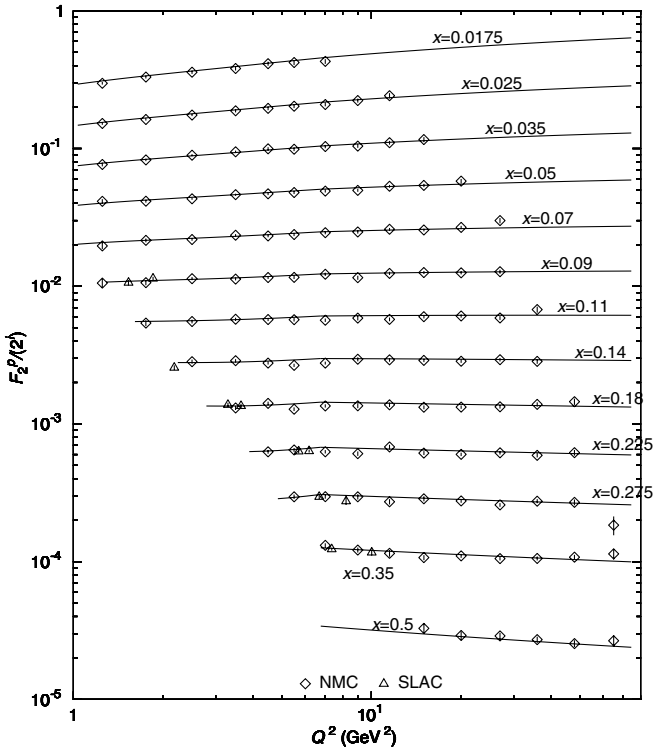

FIG. 3. DGLAP evolution results for NMC F_2^p data (the SLAC data appearing in the NMC Q^2 bins have been added to the plot). $i = 0$ for the upper curve and is increased by 1 from one curve to the next one.

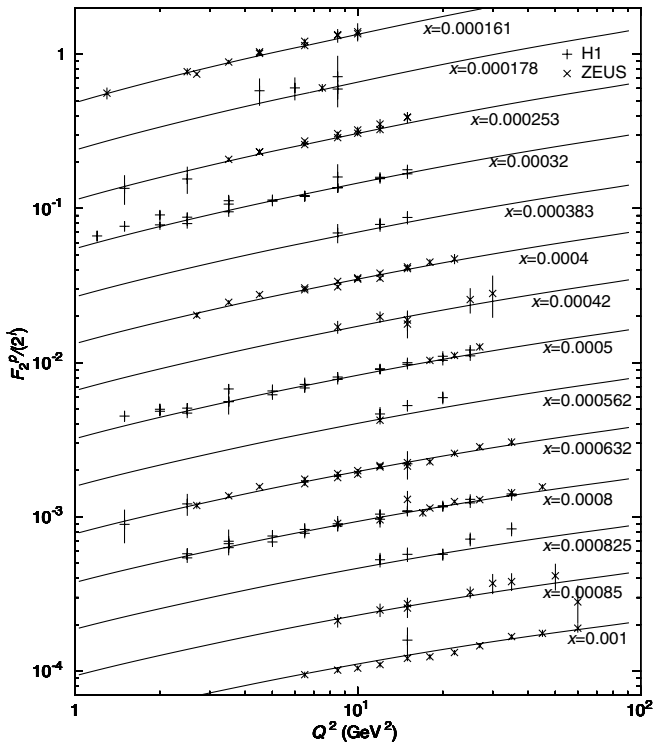

FIG. 4. DGLAP evolution results for HERA F_2^p data ($x \leq 0.001$). $i = 0$ for the upper curve and is increased by 1 from one curve to the next one.

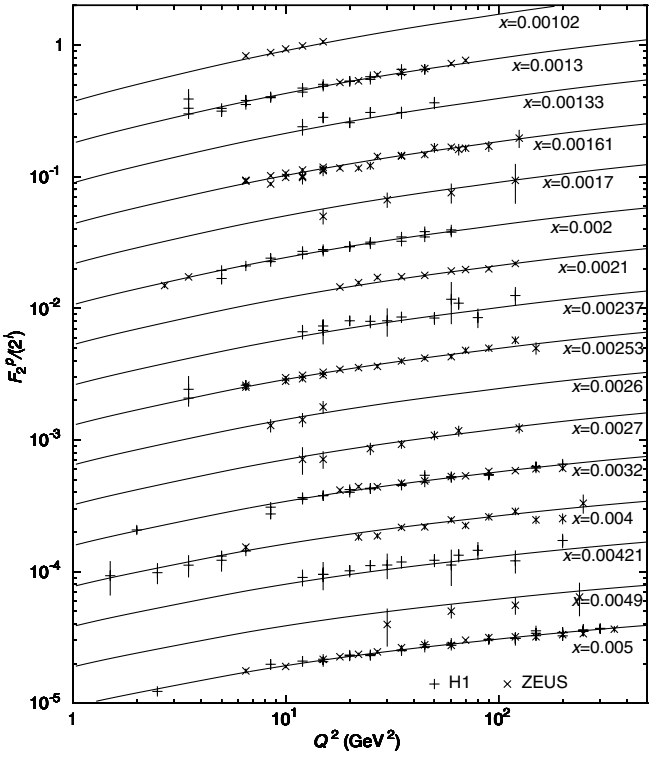

FIG. 5. DGLAP evolution results for HERA F_2^p data ($0.001 < x \leq 0.005$). $i = 0$ for the upper curve and is increased by 1 from one curve to the next one.

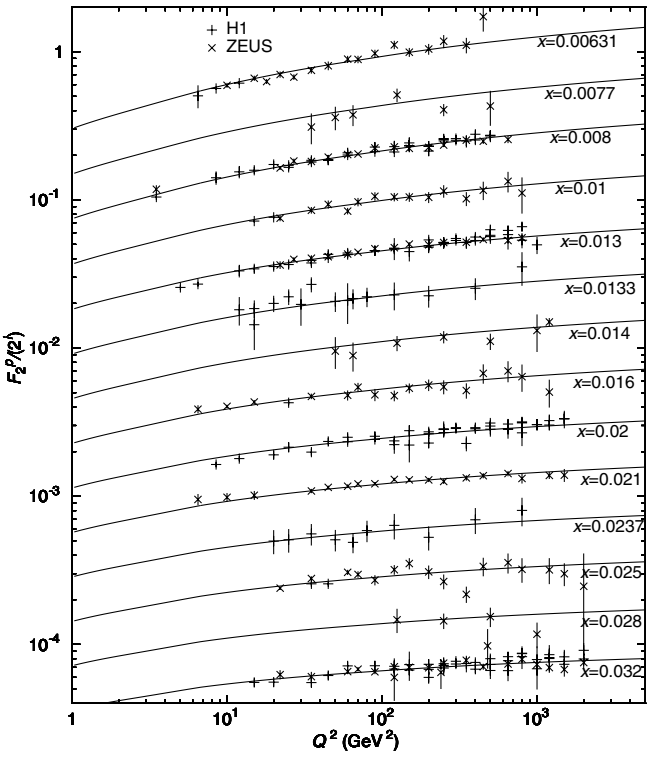

FIG. 6. DGLAP evolution results for HERA F_2^p data ($0.005 < x \leq 0.04$). $i = 0$ for the upper curve and is increased by 1 from one curve to the next one.

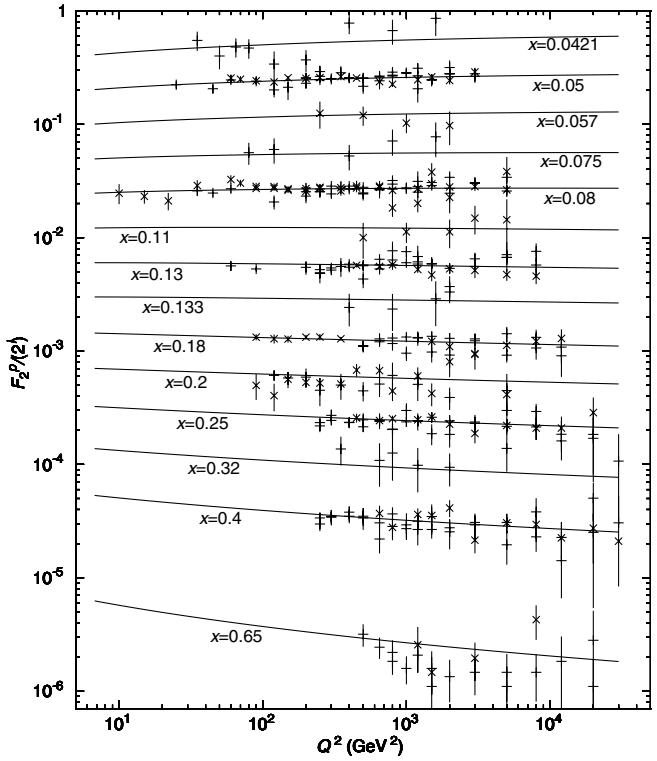

FIG. 7. DGLAP evolution results for HERA F_2^p data ($0.04 < x$). $i = 0$ for the upper curve and is increased by 1 from one curve to the next one.

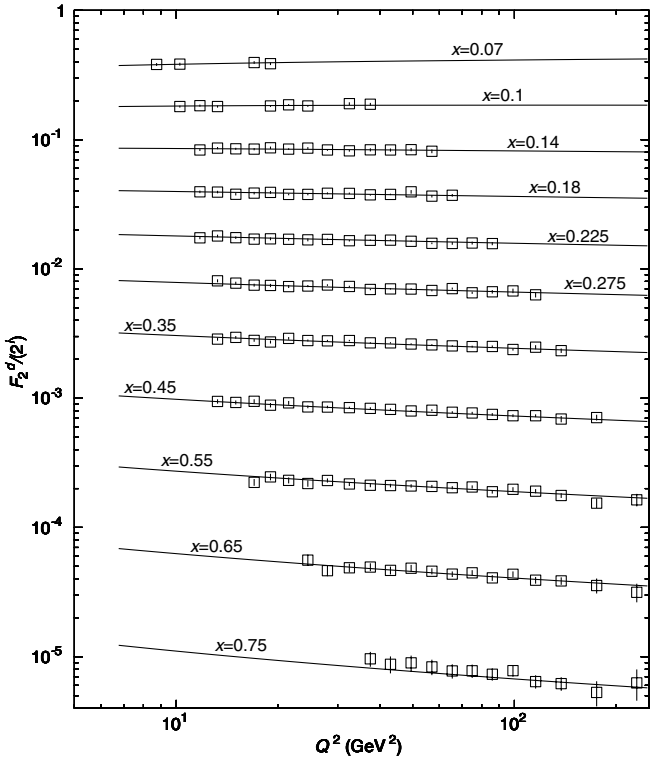

FIG. 8. DGLAP evolution results for BCDMS F_2^d data. $i = 0$ for the upper curve and is increased by 1 from one curve to the next one.

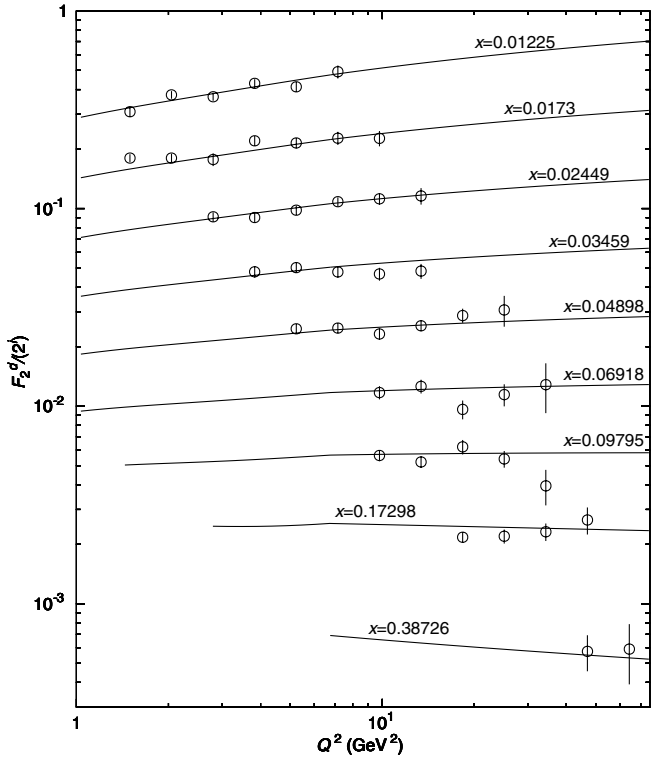

FIG. 9. DGLAP evolution results for E665 F_2^d data. $i = 0$ for the upper curve and is increased by 1 from one curve to the next one.

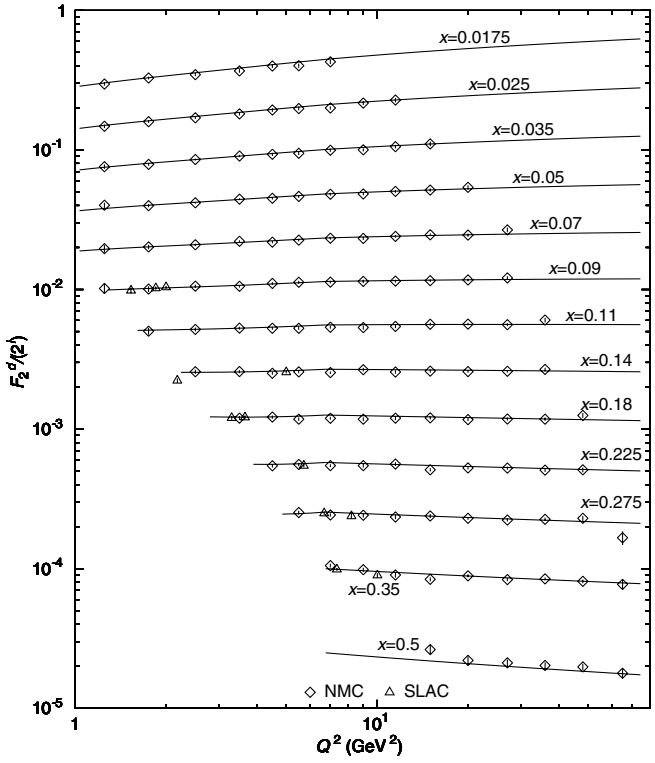

FIG. 10. DGLAP evolution results for NMC F_2^d data (the SLAC data appearing in the NMC Q^2 bins have been added to the plot). $i = 0$ for the upper curve and is increased by 1 from one curve to the next one.

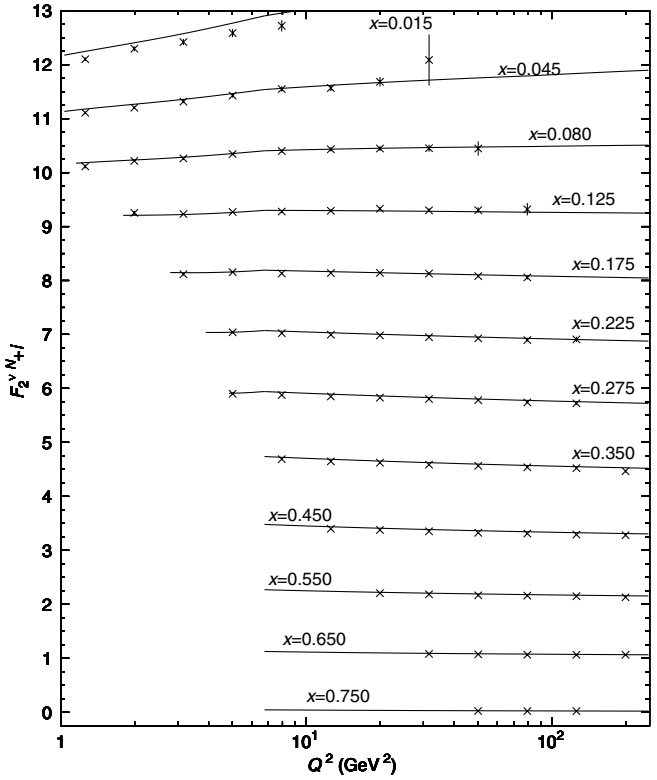

FIG. 11. DGLAP evolution results for CCFR $F_2^{\nu N}$ data. $i = 0$ for the upper curve and is increased by 1 from one curve to the next one.

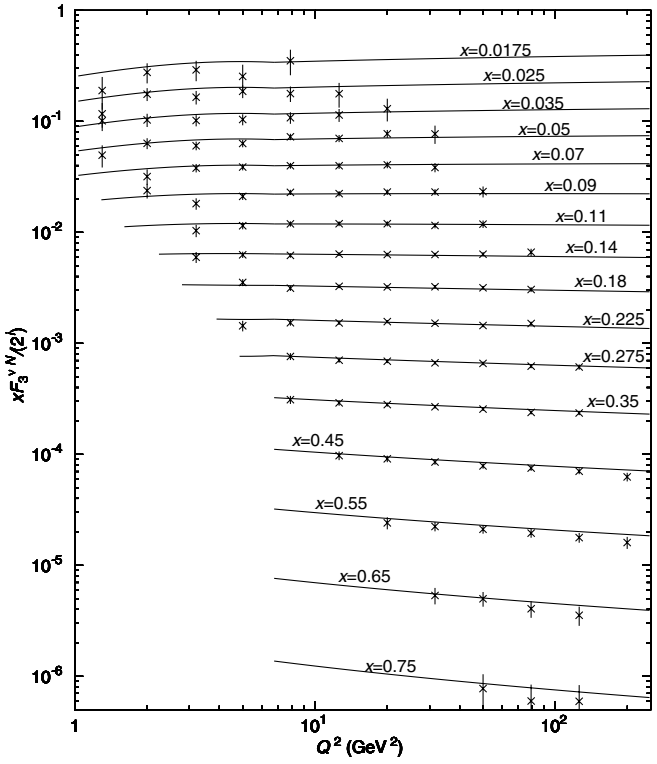

FIG. 12. DGLAP evolution results for CCFR $xF_3^{\nu N}$ data. $i = 0$ for the upper curve and is increased by 1 from one curve to the next one.

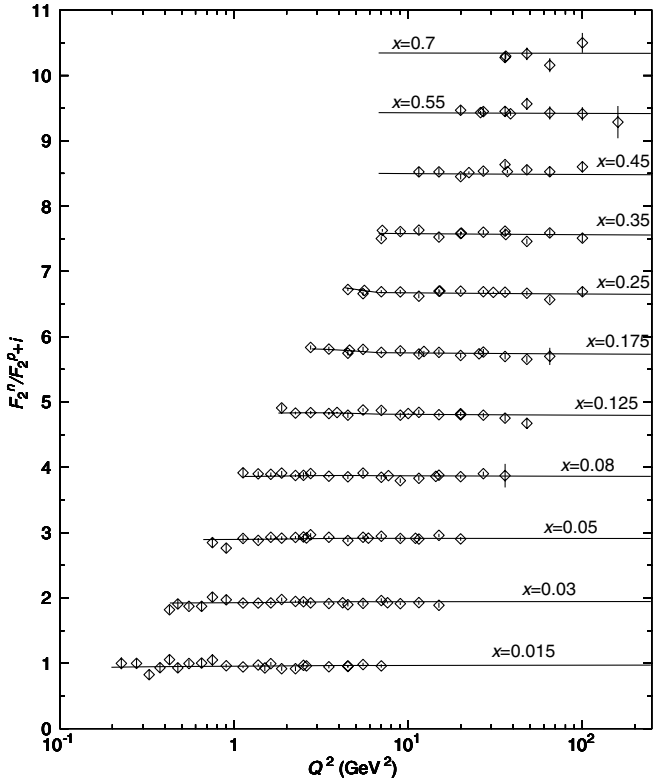

FIG. 13. DGLAP evolution results for NMC F_2^n/F_2^p data. $i = 0$ for the upper curve and is increased by 1 from one curve to the next one.

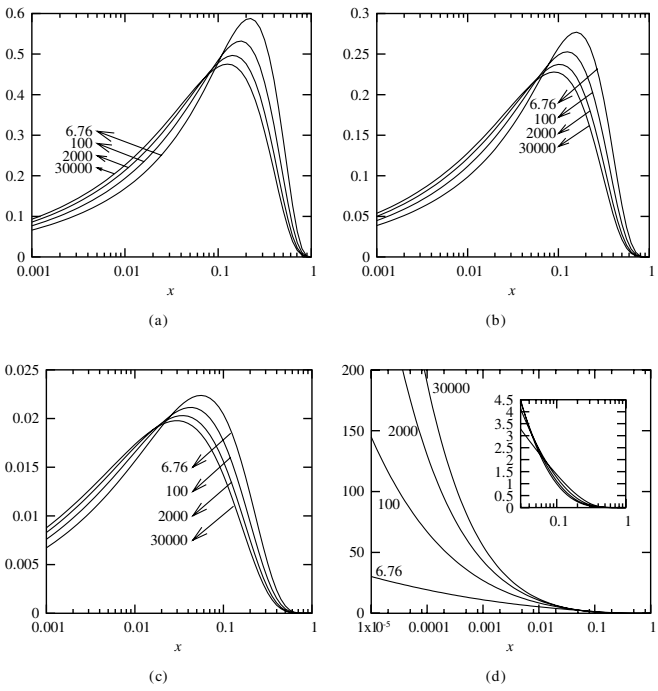

FIG. 14. Typical momentum distributions inside the proton at various Q^2: (a) u valence quarks, (b) d valence quarks, (c) sea asymmetry $\bar{d} - \bar{u}$, and (d) gluon distribution.

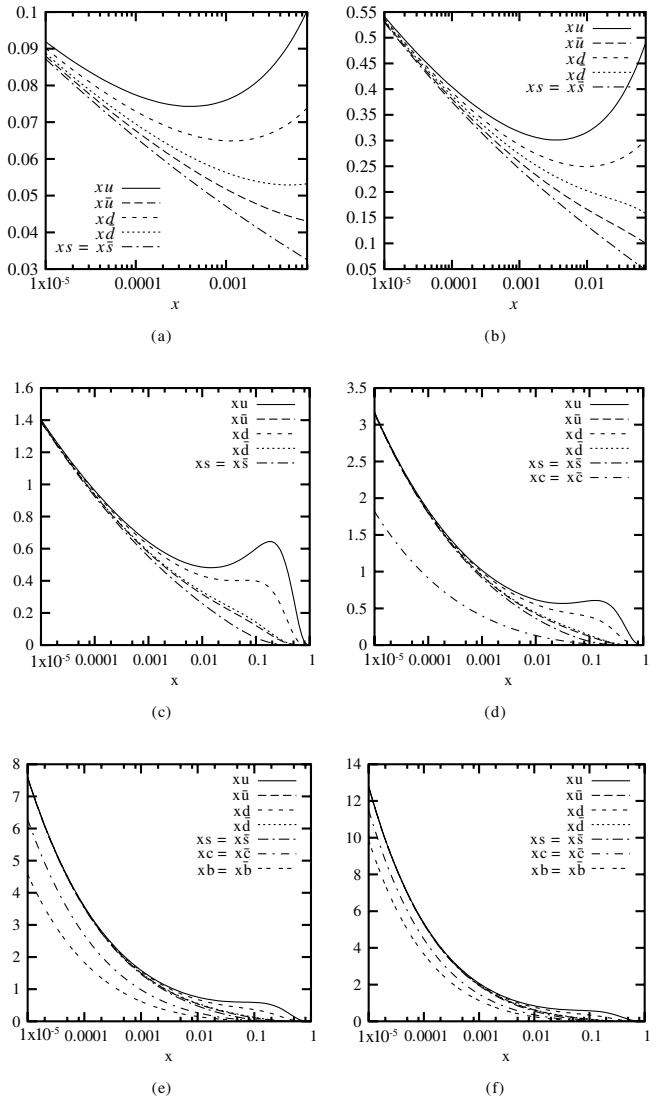

FIG. 15. Quark distributions inside the proton at various Q^2: (a) $Q^2 = 0.1$ GeV^2, (b) $Q^2 = 1$ GeV^2, (c) $Q^2 = Q_0^2 = 4m_c^2$, (d) $Q^2 = 4m_b^2$, (e) $Q^2 = 2000$ GeV^2, and (f) $Q^2 = 30\,000$ GeV^2. See VI B for details concerning the parton distributions at small Q^2.

Finally, we can estimate the uncertainty on the initial distributions in the following way: for the sea quarks or for the gluon, we have ($D = 0$ for the gluon distribution)

$$xq = [A\log^2(1/x) + B\log(1/x) + C + Dx^\eta](1-x)^b.$$

If we assume that the uncertainties on the parameters are uncorrelated, we obtain easily

$$\begin{aligned}(\delta xq)^2 = \{&\log^4(1/x)\delta A^2 + \log^2(1/x)\delta B^2 + \delta C^2 \\ &+ [\delta D^2 + \log^2(1/x)D^2\delta\eta^2]x^{2\eta} + [A\log^2(1/x) \\ &+ B\log(1/x) + C + Dx^\eta]\log^2(1-x)\delta b^2\} \\ &\times (1-x)^{2b}.\end{aligned}$$

For the valence quarks, the initial distribution has the form

$$xq_V = Kx^\eta(1-x)^b(1+\gamma x)$$

with K fixed by quark-number conservation, and we find that the uncertainty is

$$\begin{aligned}(\delta xq)^2 = K^2x^{2\eta}(1-x)^{2b}\{&[\log^4(1/x)\delta\eta^2 \\ &+ \log^2(1-x)\delta b^2](1+\gamma x)^2 + x^2\delta\gamma^2\}.\end{aligned}$$

The resulting uncertainties on the initial distributions are shown in Fig. 16, where we have also plotted the uncertainties obtained by taking into account correlations between the parameters (see Table III). We see that this ''traditional'' way of estimating errors leads to much smaller uncertainties than the joint consideration of forward and backward evolution obtained in [22].

VI. REGGE THEORY AT LOW Q^2

A. Motivation

If DGLAP evolution gives the behavior of the parton distributions at large Q^2, we expect soft physics to be

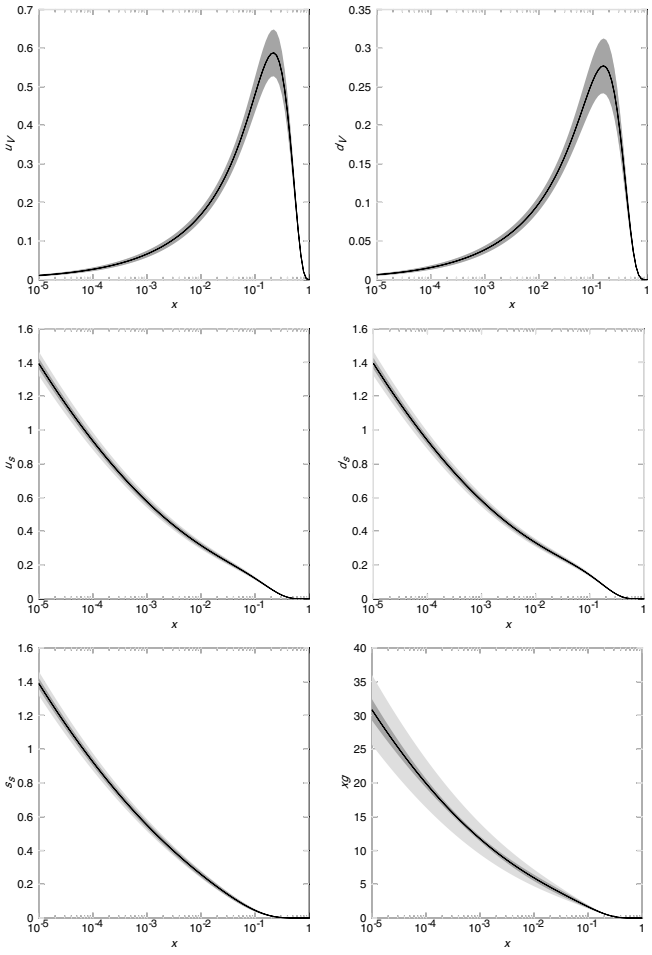

FIG. 16. Initial distributions with their uncertainties: the dark regions represent the correlated uncertainties while the light ones are obtained without taking into account the correlations between the parameters.

described by Regge theory. In other words, Regge theory should not only be able to describe the initial DGLAP condition but also the structure functions for $0 \leq Q^2 \leq Q_0^2$. In this section, we shall therefore try to extend the parton distribution functions at low values of Q^2. Note that in this region, we cannot use the DGLAP equation anymore. In addition, if we want to use Regge theory, we must still restrict ourselves to the high-energy domain. Hence we keep the constraint

$$W^2 \geq 12.5 \text{ GeV}^2$$

but allow Q^2 to be in the region

$$0 \leq Q^2 \leq 6.76 \text{ GeV}^2.$$

B. Small-Q^2 parametrization

If we want to use Regge theory in the small-Q^2 region, we need to parametrize the parton distribution functions. We shall use the same expressions as in (3) with an additional Q^2 dependence. However, if we want to consider the extension down to $Q^2 = 0$, we know that we should use the Regge variable $\nu = \frac{Q^2}{2x}$ instead of x. This means that we shall use the following distributions:

$$xu_V(\nu, Q^2) = \frac{2}{N_u^*}(2\nu)^{-\eta}\left[1 + \gamma_u(Q^2)\frac{Q^2}{2\nu}\right]\left(1 - \frac{Q^2}{2\nu}\right)^{b_u(Q^2)}, \tag{4}$$

$$xd_V(\nu, Q^2) = \frac{1}{N_d^*}(2\nu)^{-\eta}\left[1 + \gamma_d(Q^2)\frac{Q^2}{2\nu}\right]\left(1 - \frac{Q^2}{2\nu}\right)^{b_d(Q^2)},$$

$$xu_s(\nu, Q^2) = \{\mathcal{A}(Q^2)[\log(2\nu) - \mathcal{B}(Q^2)]^2 + C(Q^2) + \mathcal{D}_u(Q^2)(2\nu)^{-\eta}\}\left(1 - \frac{Q^2}{2\nu}\right)^{b(Q^2)},$$

$$xd_s(\nu, Q^2) = \{\mathcal{A}(Q^2)[\log(2\nu) - \mathcal{B}(Q^2)]^2 + C(Q^2) + \mathcal{D}_d(Q^2)(2\nu)^{-\eta}\}\left(1 - \frac{Q^2}{2\nu}\right)^{b(Q^2)},$$

$$xs_s(\nu, Q^2) = \{\mathcal{A}(Q^2)[\log(2\nu) - \mathcal{B}(Q^2)]^2 + C(Q^2) + \mathcal{D}_s(Q^2)(2\nu)^{-\eta}\}\left(1 - \frac{Q^2}{2\nu}\right)^{b(Q^2)},$$

where, once again, N_u and N_d are constrained by quark-number conservation. We shall require that the parameters in these distributions match the initial distribution taken for DGLAP evolution at 6.76 GeV^2. Using parametrizations of the form[11]

$$\phi(Q^2) = a_\phi Q^2\left(\frac{Q_\phi^2}{Q^2 + Q_\phi^2}\right)^{\varepsilon_\phi} \quad \text{for } \phi = \mathcal{A}, C, \mathcal{D}_u, \mathcal{D}_d, b, b_u, b_d, \qquad \mathcal{B}(Q^2) = a_\mathcal{B}\left(\frac{Q^2}{Q^2 + Q_\mathcal{B}^2}\right)^{\varepsilon_\mathcal{B}} + a_\mathcal{B}^*,$$

$$\gamma_i(Q^2) = \gamma_i(Q_0^2) \quad \text{for } i = u, d,$$

$$\mathcal{D}_s = 0$$

and constraining the parameters $a_\mathcal{A}$, $a_\mathcal{B}^*$, a_C, $a_{\mathcal{D}_u}$, $a_{\mathcal{D}_d}$, $a_{\mathcal{D}_s}$, a_b, a_{b_u}, and a_{b_d} with the DGLAP initial condition at $Q^2 = Q_0^2 = 6.76$ GeV^2, we are left with 17 parameters: $a_\mathcal{B}$, $Q_\mathcal{A}^2$, $Q_\mathcal{B}^2$, Q_C^2, $Q_{\mathcal{D}_u}^2$, $Q_{\mathcal{D}_d}^2$, Q_b^2, $Q_{b_u}^2$, $Q_{b_d}^2$, $\varepsilon_\mathcal{A}$, $\varepsilon_\mathcal{B}$, ε_C, $\varepsilon_{\mathcal{D}_u}$, $\varepsilon_{\mathcal{D}_d}$, ε_b, ε_{b_u}, and ε_{b_d}. The expressions obtained once the constrained have been imposed are the following:

$$\mathcal{A}(Q^2) = A\frac{Q^2}{Q_0^2} * \left(\frac{Q_0^2 + Q_\mathcal{A}^2}{Q^2 + Q_\mathcal{A}^2}\right)^{\varepsilon_\mathcal{A}},$$

$$\mathcal{B}(Q^2) = a_\mathcal{B}\left[\left(\frac{Q^2}{Q^2 + Q_\mathcal{B}^2}\right)^{\varepsilon_\mathcal{B}} - \left(\frac{Q_0^2}{Q_0^2 + Q_\mathcal{B}^2}\right)^{\varepsilon_\mathcal{B}}\right] + \log(Q_0^2) - \frac{B}{2A},$$

$$C(Q^2) = \left(C - \frac{B^2}{4A}\right)\frac{Q^2}{Q_0^2}\left(\frac{Q_0^2 + Q_C^2}{Q^2 + Q_C^2}\right)^{\varepsilon_C},$$

$$\mathcal{D}_u(Q^2) = D_u\frac{Q^2}{Q_0^2}(Q_0^2)^\eta\left(\frac{Q_0^2 + Q_{\mathcal{D}_u}^2}{Q^2 + Q_{\mathcal{D}_u}^2}\right)^{\varepsilon_{\mathcal{D}_u}},$$

$$\mathcal{D}_d(Q^2) = D_d\frac{Q^2}{Q_0^2}(Q_0^2)^\eta\left(\frac{Q_0^2 + Q_{\mathcal{D}_d}^2}{Q^2 + Q_{\mathcal{D}_d}^2}\right)^{\varepsilon_{\mathcal{D}_d}},$$

$$\mathcal{D}_s(Q^2) = 0,$$

$$b(Q^2) = b\frac{Q^2}{Q_0^2} * \left(\frac{Q_0^2 + Q_b^2}{Q^2 + Q_b^2}\right)^{\varepsilon_b},$$

$$b_u(Q^2) = b_u\frac{Q^2}{Q_0^2} * \left(\frac{Q_0^2 + Q_{b_u}^2}{Q^2 + Q_{b_u}^2}\right)^{\varepsilon_{b_u}},$$

$$b_d(Q^2) = b_d\frac{Q^2}{Q_0^2} * \left(\frac{Q_0^2 + Q_{b_d}^2}{Q^2 + Q_{b_d}^2}\right)^{\varepsilon_{b_d}},$$

$$\gamma_u(Q^2) = \gamma_u,$$

$$\gamma_d(Q^2) = \gamma_d.$$

[11] Since $\mathcal{D}_s$ already vanishes at $Q^2 = Q_0^2$, we have set it to zero in the whole small-Q^2 region.

TABLE III. Fitted parameters correlation coefficients.

Parameter	Global	A	B	C	D_u	D_d	D_s	A_g	B_g	γ_u	γ_d	b_u	b_d	b	η
A	0.996 50	1.000	−0.895	−0.015	0.733	0.631	0.007	−0.363	0.268	0.365	0.304	0.018	−0.022	0.442	−0.368
B	0.998 24	−0.895	1.000	0.025	−0.864	−0.668	−0.006	0.229	−0.148	−0.567	−0.494	−0.081	−0.042	−0.589	0.562
C	0.289 80	−0.015	0.025	1.000	0.005	0.005	0.000	0.001	−0.002	0.001	0.001	0.001	0.000	0.000	0.002
D_u	0.992 22	0.733	−0.864	0.005	1.000	0.822	0.006	0.086	−0.177	0.524	0.521	0.267	0.085	0.876	−0.460
D_d	0.982 33	0.631	−0.668	0.005	0.822	1.000	0.005	−0.071	−0.009	0.110	0.040	0.397	−0.243	0.762	−0.009
D_s	0.026 47	0.007	−0.006	0.000	0.006	0.005	1.000	0.001	−0.002	0.005	0.005	0.004	0.000	0.008	−0.004
A_g	0.996 16	−0.363	0.229	0.001	0.086	−0.071	0.001	1.000	−0.980	0.346	0.380	0.253	0.199	0.356	−0.291
B_g	0.996 49	0.268	−0.148	−0.002	−0.177	−0.009	−0.002	−0.980	1.000	−0.403	−0.443	−0.317	−0.228	−0.464	0.332
γ_u	0.999 56	0.365	−0.567	0.001	0.524	0.110	0.005	0.346	−0.403	1.000	0.900	0.253	0.318	0.518	−0.980
γ_d	0.996 65	0.304	−0.494	0.001	0.521	0.040	0.005	0.380	−0.443	0.900	1.000	0.081	0.648	0.552	−0.893
b_u	0.974 69	0.018	−0.081	0.000	0.267	0.397	0.004	0.253	−0.317	0.253	0.081	1.000	−0.232	0.537	−0.073
b_d	0.973 29	−0.022	−0.042	0.000	0.085	−0.243	0.000	0.199	−0.228	0.318	0.648	−0.232	1.000	0.174	−0.332
b	0.996 85	0.442	−0.589	0.002	0.876	0.762	0.008	0.356	−0.464	0.518	0.552	0.537	0.174	1.000	−0.389
η	0.999 65	−0.368	0.562	−0.001	−0.460	−0.009	−0.004	−0.291	0.332	−0.980	−0.893	−0.073	−0.332	−0.389	1.000

C. Data set and systematic errors

In the small-Q^2 region ($W^2 \geq 12.5$ GeV^2, $Q^2 \leq 6.76$ GeV^2), we shall fit the same quantities as previously and the data coming from the same collaborations:

(i) F_2^p: H1 [26–28,31], ZEUS [34–39], NMC [42], E665 [41], SLAC [43],
(ii) F_2^d: BCDMS, NMC [42], E665 [41], SLAC [51],
(iii) F_2^n/F_2^p: NMC [48],
(iv) $F_2^{\nu N}$ and $xF_3^{\nu N}$: CCFR [47].

Concerning the treatment of the systematic errors, we have used the same correction factors as the ones obtained in the DGLAP global fit for the papers containing data in both the small- and the large-Q^2 regions and leave this factor free for the papers containing only data at small Q^2.

D. Results

The parametrizations described above have been fitted to the 948 data in the small-Q^2 region using MINUIT. The results of this fit, experiments by experiments, together with the parameter values are presented in Tables IV and V. We see that, apart from the ZEUS 1995 data and the CCFR F_2 data, we obtain a good description of the structure functions in the low-Q^2 region. The χ^2 per data point is quite good, considering that we have applied Regge theory to quite a large region as compared to the usual approaches [17,19,23,52–54]. The poor description of the ZEUS 1995 data may come from the fact that the systematic uncertainties have been fixed in the DGLAP fit.

The results for the structure functions in the low-Q^2 region are shown in Figs. 1–13 together with the large-Q^2 results. In the small-Q^2 region, the curves are drawn only in the fitted region ($W^2 > 12.5$ GeV^2). We see that the experimental measurements are well reproduced.

Finally, the curves in Fig. 15 show the parton distribution functions obtained at small Q^2. It is interesting to notice that valence quarks are large at small Q^2 and $W^2 \approx 12.5$ GeV^2 which, in this case, corresponds to small values of x. For example, at $Q^2 = 0.1$ GeV^2 and $x = 0.008$, we have $x\bar{u} \approx 0.043$, $x\bar{d} \approx 0.053$, $xu_V \approx 0.057$, and $xd_V \approx 0.019$. It is also interesting to point out that, in the limit $Q^2 = 0$, i.e. the total cross-section limit, $x = \frac{Q^2}{2\nu}$ goes to 0. Thus, as explicitly seen from Eq. (A1), the powers of $1 - x$ have no effects on the description of the total cross section which involves only pomeron and Reggeons terms. This is consistent with the energy cut $W^2 \geq 12.5$ GeV^2 which removes the resonance region in the total cross sections. The same argument also holds for the resonance region in fixed target data which requires not only a more complete Regge description but also a treatment of higher-twist effects from the point of view of DGLAP evolution.

VII. DGLAP VS REGGE AT HIGH Q^2

A. Motivation

As we have shown in [22], we can consider the fact that Regge theory also applies at large Q^2. In these conditions, since Q^2-dependent singularities are forbidden in Regge theory, we expect a triple-pole behavior at all values of Q^2. The unphysical essential singularity generated by DGLAP evolution should therefore be considered as a numerical approximation to a triple-pole pomeron at small x.

Given these considerations, we have shown [22] that, using both forward and backward evolutions, it is possible to describe the small-x experimental data with parton distribution functions of the form

$$A(Q^2)\log^2(1/x) + B(Q^2)\log(1/x) + C(Q^2) + D(Q^2)x^\eta$$

where the Q^2-dependent couplings are extracted from the DGLAP evolution equation.

B. Parametrization and uncertainties

In this QCD global fit, we would like to test if it is still possible to consider the result of the evolution as an approximation to a triple pole. To achieve this task, we shall fit the parton distribution functions at each value of Q^2 with the following form:

TABLE IV. Result of the small-Q^2 fit detailed experiment by experiment. We also give the result of the large Q^2 fit as given in Table II and the combined results.

Experiment information				Small Q^2		Large Q^2		Total	
Quant.	Collab.	Reference	Norm.	nop	χ^2/nop	nop	χ^2/nop	nop	χ^2/nop
F_2^p	E665	PRD54(1996)3006	1.80	61	0.906	30	1.346	91	1.051
	H1	NPB439(1995)471	−4.50	3	0.278	90	0.550	93	0.541
		NPB470(1996)3	···	37	0.419	156	0.688	193	0.620
		NPB497(1996)3	−3.00	44	0.810	···	···	44	0.810
		EPJC21(2001)33	···	47	1.313	86	0.881	133	1.034
		NPB407(1993)515	−8.00	···	···	21	0.297	21	0.297
		EPJC13(2000)609	−1.50	···	···	130	0.905	130	0.905
		EPJC19(2001)269	−1.50	···	···	126	1.029	126	1.029
	NMC	NPB483(1997)3	2.10	67	0.694	79	1.290	146	1.016
	SLAC	PLB282(1992)475	···	94	1.090	52	1.882	146	1.372
	ZEUS	ZPC69(1995)607	−1.54	14	2.104	9	1.277	23	1.780
		ZPC72(1996)399	···	16	0.709	172	1.389	188	1.331
		PLB407(1997)432	···	34	0.316	···	···	34	0.316
		EPJC7(1999)609	···	32	1.079	12	0.941	44	1.042
		EPJC12(2000)35	···	70	1.230	···	···	70	1.230
		EPJ21(2001)443	···	28	1.716	214	0.969	242	1.055
		PLB316(19931)412	6.94	···	···	17	0.356	17	0.356
		ZPC65(1995)379	2.00	···	···	56	0.491	56	0.491
	BCDMS	PLB223(1989)485	···	···	···	167	0.926	167	0.926
	Total		···	547	0.984	1417	0.974	1964	0.977
F_2^d	E665	PRD54(1996)3006	···	61	1.262	30	1.119	91	1.215
	NMC	NPB483(1997)3	1.00	67	0.598	79	1.143	146	0.893
	SLAC	SLAC-357(1990)	···	98	0.883	50	1.968	148	1.249
		PRD49(1994)5641	0.89	1	0.000	···	···	1	0.000
	BCDMS	PLB237(1989)592	···	···	···	154	0.831	154	0.831
	Total		···	227	0.897	313	1.119	540	1.025
$F_2^{\nu N}$	CCFR	Yang's thesis	3.00	19	3.325	65	2.546	84	2.722
$xF_3^{\nu N}$	CCFR	PRL79(1997)1213	···	35	1.120	76	0.554	111	0.732
F_2^n/F_2^p	NMC	NPB371(1995)3	···	120	0.845	91	1.283	211	1.034
Total			···	948	0.997	1962	1.047	2910	1.031

TABLE V. Value of the parameters with their errors for the low-Q^2 fit. The scales are given in GeV^2.

Parameter	Value	Error
$a_{\mathcal{B}}$	15.05	1.80
$Q^2_{\mathcal{A}}$	6.37	2.72
$Q^2_{\mathcal{B}}$	1.885	0.522
Q^2_C	10.00	8.70
$Q^2_{\mathcal{D}_u}$	0.437	1.07
$Q^2_{\mathcal{D}_d}$	5.19	3.11
Q^2_b	3.64	1.87
$Q^2_{b_u}$	5.10	2.38
$Q^2_{b_d}$	87.9	15.8
$\varepsilon_{\mathcal{A}}$	1.002	0.328
$\varepsilon_{\mathcal{B}}$	0.581	0.110
ε_C	18.19	4.37
$\varepsilon_{\mathcal{D}_u}$	0.340	0.157
$\varepsilon_{\mathcal{D}_d}$	1.618	0.615
ε_b	1.916	0.453
ε_{b_u}	2.558	0.593
ε_{b_d}	10.00	6.94

$$xu_V = \frac{2}{N_u^*} x^\eta (1 + \gamma_u x)(1 - x)^{b_u},$$

$$xd_V = \frac{1}{N_d^*} x^\eta (1 + \gamma_d x)(1 - x)^{b_d},$$

$$xu_s = [A \log^2(1/x) + B \log(1/x) + C + D_u x^\eta](1 - x)^b,$$

$$xd_s = [A \log^2(1/x) + B \log(1/x) + C + D_d x^\eta](1 - x)^b,$$

$$xs_s = N_s[A \log^2(1/x) + B \log(1/x) + C + D_s x^\eta] \times (1 - x)^b,$$

$$xc_s = N_c[A \log^2(1/x) + B \log(1/x) + C + D_c x^\eta] \times (1 - x)^b,$$

$$xb_s = N_b[A\log^2(1/x) + B\log(1/x) + C + D_b x^\eta] \times (1-x)^b.$$

$$xg = [A_g\log^2(1/x) + B_g\log(1/x) + C_g^*](1-x)^{b+1}.$$

Before performing this fit, we shall determine an uncertainty on the parton distribution. Since we want to show that the DGLAP evolution generates an essential singularity which mimics a triple-pole behavior, we should estimate the error introduced by the evolution. Since we have used LO DGLAP evolution, we estimate that the errors are of the order of the NLO corrections:

$$q_{\mathrm{NLO}}(x, Q^2) \approx (1 \pm \alpha_s(Q^2))q_{\mathrm{LO}}(x, Q^2).$$

If we require that the initial parton distribution at $Q^2 = Q_0^2$ remains fixed, this leads to

$$q_{\mathrm{NLO}}^{\mathrm{norm}}(x, Q^2) \approx \frac{1 \pm \alpha_s(Q^2)}{1 \pm \alpha_s(Q_0^2)} q_{\mathrm{LO}}(x, Q^2),$$

or, keeping only the leading term in the strong coupling constant,

$$\Delta q(x, Q^2) = |\alpha_s(Q_0^2) - \alpha_s(Q^2)| q_{\mathrm{LO}}(x, Q^2).$$

In addition, we shall take into account the fact that, at small Q^2, there may also be higher-twist corrections. If we assume[12] these are at 5% at $Q^2 = Q_0^2$, we shall finally consider

$$\Delta q(x, Q^2) = \left[|\alpha_s(Q_0^2) - \alpha_s(Q^2)| + \frac{0.05 Q_0^2}{(1-x)Q^2} \right] q_{\mathrm{LO}}(x, Q^2).$$

Finally, additional powers of $1 - x$ are expected to describe the large-x behavior of the parton distributions at large Q^2, hence we shall consider only the region $10^{-5} \leq x \leq 0.1$ for the sea quarks and the gluons. For the case of the valence quarks, we hope that the factor $(1 + \gamma x)$ is sufficient to reproduce the distribution for $10^{-5} \leq x \leq 1$.

C. Results

To perform the fit, we have taken the parton distributions with their estimated uncertainties in 80 points regularly spaced in $\log(x)$. Since the parametrizations for the valence quarks and the sea quarks have disjoint parameters, we have performed two different fits at each Q^2. The results of these are presented in Fig. 17 for $Q^2 = 100\ \mathrm{GeV}^2$ and $Q^2 = 10\,000\ \mathrm{GeV}^2$. In addition, the predictions for the triple-pole residues for F_2^p are shown in Fig. 18 together with the χ^2 per point of the fit.

We clearly see that the parametrization works very well for valence quarks at all values of Q^2, as well as for the u_s and d_s distributions. For heavy quarks and gluons, although the χ^2 per data point remains less than 1, there are some discrepancies between the DGLAP essential singularity and the triple-pole fit at small x and large Q^2. However, these differences are present only for $\sqrt{s} > 3\,\mathrm{TeV}$, which means that it is impossible to distinguish between the two approaches in present experimental measurements. This high-energy region should be reached at the LHC and should provide very useful information to distinguish between the different models.

Moreover, we have also tried to estimate the uncertainties on the parton densities in another way. We have considered the uncertainties obtained from the DGLAP fit at $Q^2 = Q_0^2$:

$$q(x, Q_0^2) - \Delta q(x, Q_0^2) \leq q(x, Q_0^2) \leq q(x, Q_0^2) + \Delta q(x, Q_0^2).$$

We can then evolve $q(x, Q_0^2) \pm \Delta q(x, Q_0^2)$ and using these quantities to obtain the uncertainties at all values of Q^2. If we do so, we obtain very similar conclusions.

VIII. CONCLUSIONS AND PERSPECTIVES

We have seen that we can use Regge theory to constrain the initial parton densities at $Q^2 = Q_0^2$ and obtain the distributions at higher virtualities with the DGLAP evolution equation. In this approach, Regge theory is used to describe the low-Q^2 data and QCD applies at large Q^2. In such a way, the complex-j-plane singularities are common to parton distribution functions in the initial condition and to soft amplitudes which provides a unified description at high energy in the soft region.

We have also shown in this paper that it is possible to *define* the parton distributions in the low-Q^2 region and to parametrize them using Regge theory. This parametrization is useful to describe the DIS structure functions but should be used with care. Actually, since factorization is not proven at small Q^2, we cannot ensure that the parton distributions can be extended to $Q^2 = 0$. Using our parametrization to describe processes such as jet production may be incorrect.

Considering the low-Q^2 parametrization together with the global QCD fit, we have a combined description of the hadronic structure functions over the whole Q^2 range. This model, consistent with DGLAP evolution and with Regge theory, reproduces the experimental measurements with a very good χ^2.

In addition, we extended the approach of [20] to $x = 1$ using only forward evolution. We have not applied the techniques developed in [22] and extracted the Q^2 behavior of the fitted parameters by combining forward and backward evolution. The reason is that, even with a few parameters, there often exist multiple minima and it is quite hard to obtain a continuous result for all parameters. This situation is expected to be even worse with the parametri-

[12]This value reproduces errors comparable with those obtained from our uncertainties estimation. In addition, the higher-twist term is relevant for middle-range values of Q^2 while the subleading corrections are important at large Q^2.

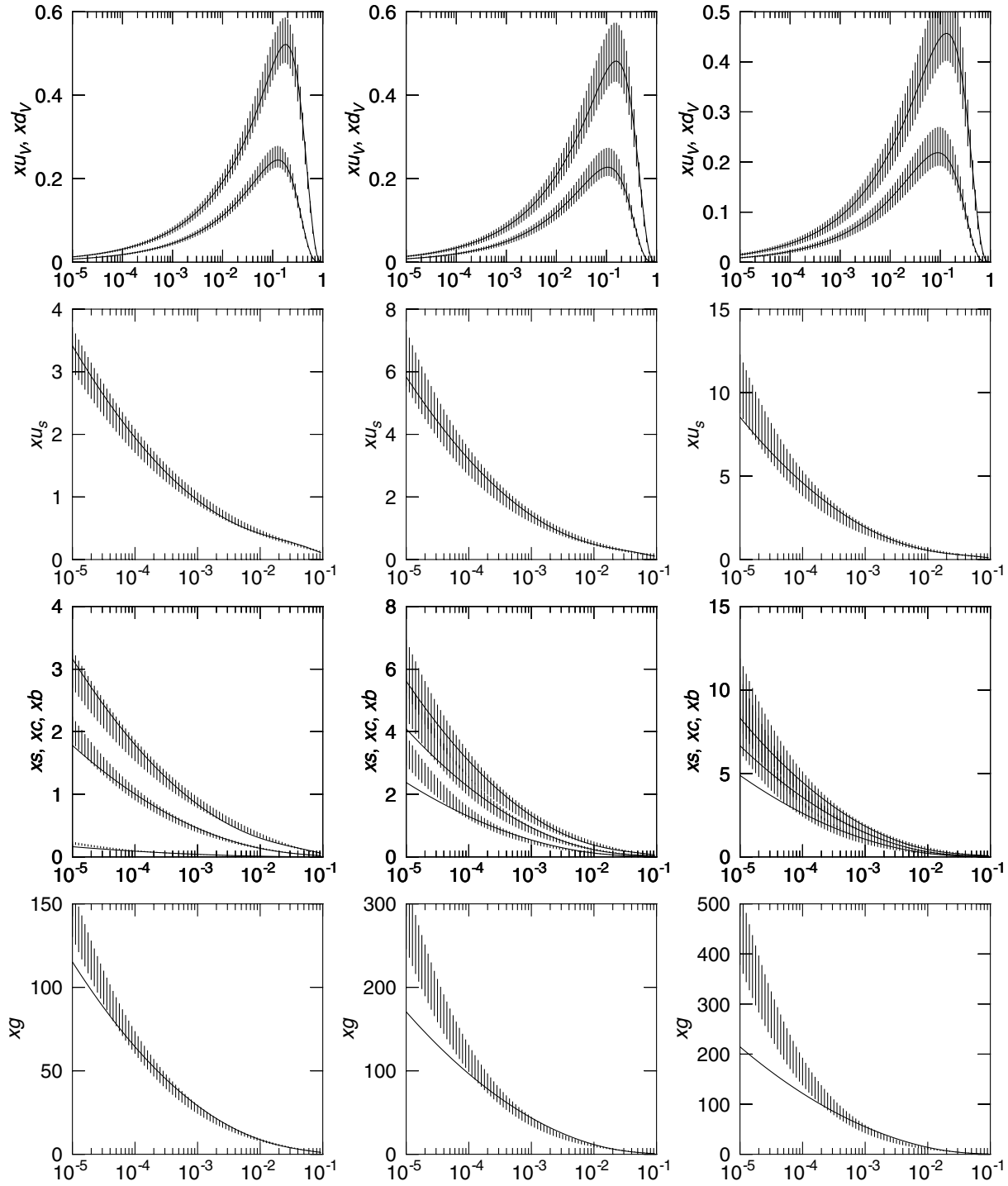

FIG. 17. Triple-pole pomeron fit to the parton distribution functions obtained from DGLAP evolution. The first column shows distributions at $Q^2 = 100$ GeV^2, the second corresponds to $Q^2 = 1000$ GeV^2, and the third to $Q^2 = 10\,000$ GeV^2.

zation used here due to the larger number of parameters. Hence, in order to test the compatibility between the DGLAP-evolved parton distributions and a triple-pole parametrization, we have shown that the parton densities can be approximated by a $\log^2(1/x)$ behavior at small x and large Q^2. This approximation works very well up to $\sqrt{s} \approx 3$ TeV, and at which point it deviates from DGLAP for the heavy quarks and the gluons. This means that we expect high-energy corrections to be important in this domain and that the CERN LHC should provide very useful information to distinguish between the different high-energy models. In this high-energy region, one should expect contributions from the BFKL equation as well as unitarity and saturation effects.

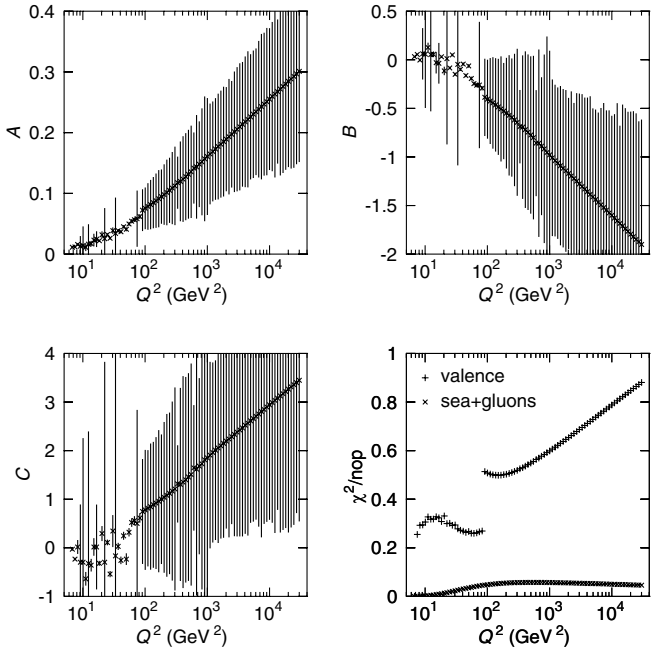

FIG. 18. Triple-pole form factors for F_2^p at large Q^2 presented together with the result of the fit of a triple-pole to the large-Q^2 parton densities.

Finally, a NLO analysis will be performed in the near future. This gives a much more reliable description of the data, allows a more complete comparison with other parametrizations, and gives a description of the F_c and F_L structure functions.

ACKNOWLEDGMENTS

First of all, I would like to thank J. R. Cudell for very useful discussions and suggestions. I am also very grateful to L. Favart and J. Stirling. Finally, I would like to thank Y. K. Yang for fruitful discussions concerning the CCFR measurements. This work is supported by the National Fund for Scientific Research (FNRS), Belgium.

APPENDIX: MOMENTUM SUM RULE AND GLUON DISTRIBUTION

In this Appendix, we shall give the expression of the constant in the gluon distribution, constrained by the momentum sum rule. Recall that we have, at $Q^2 = Q_0^2$,

$$\begin{aligned} xu_V(x) &= \frac{2}{N_u} x^\eta (1+\gamma_u x)(1-x)^{b_u}, \\ xd_V(x) &= \frac{1}{N_d} x^\eta (1+\gamma_d x)(1-x)^{b_d}, \\ x\bar{q}_i(x) &= [A\log^2(1/x) + B\log(1/x) + C + D_i x^\eta] \\ &\quad \times (1-x)^b, \\ xg(x) &= [A_g \log^2(1/x) + B_g \log(1/x) + C_g](1-x)^{b+1}, \end{aligned} \tag{A1}$$

where N_q is given by Eq. (2). We shall use momentum conservation to constrain the constant term C_g in the gluon distribution. Let us first introduce the special functions that we need. The Euler gamma function is defined by

$$\Gamma(x) = \int_0^\infty dt t^{x-1} e^{-t}.$$

We can then introduce the beta function $B(x, y)$, the digamma function $\Psi(x)$, and the polygamma function $\Psi^{(m)}(x)$ related to the gamma functions by the following formulas:

$$B(x, y) = \frac{\Gamma(x)\Gamma(y)}{\Gamma(x+y)},$$

$$\Psi(x) = \frac{\partial_x \Gamma(x)}{\Gamma(x)},$$

$$\Psi^{(m)}(x) = \partial_x^m \Psi(x).$$

With these definitions, the momenta carried by the distributions (A1) are given by the following expressions:

$$\begin{aligned} p_{u_V} &= \frac{2\eta}{b_u+\eta+1}\left(1+\gamma_u \frac{\eta+1}{b_u+\eta+2}\right) \\ &\quad \times \left(1+\gamma_u \frac{\eta}{b_u+\eta+1}\right)^{-1}, \end{aligned}$$

$$\begin{aligned} p_{d_V} &= \frac{\eta}{b_d+\eta+1}\left(1+\gamma_d \frac{\eta+1}{b_d+\eta+2}\right) \\ &\quad \times \left(1+\gamma_d \frac{\eta}{b_d+\eta+1}\right)^{-1}, \end{aligned}$$

$$\begin{aligned} p_{\bar{q}_i} &= \frac{1}{b+1}\left(A\left\{\left[\gamma_E + \Psi(b+2)\right]^2 - \Psi^{(1)}(b+2) + \frac{\pi^2}{6}\right\}\right. \\ &\quad \left. + B[\gamma_E + \Psi(b+2)] + C\right) + D_i B(b+1, \eta+1), \end{aligned}$$

$$\begin{aligned} p_g &= \frac{1}{b_g+1}\left(A_g\left\{[\gamma_E + \Psi(b_g+2)]^2 - \Psi^{(1)}(b_g+2)\right.\right. \\ &\quad \left.\left. + \frac{\pi^2}{6}\right\} + B_g[\gamma_E + \Psi(b_g+2)] + C_g\right). \end{aligned}$$

From the proton, momentum conservation gives

$$p_g + p_{u_V} + p_{d_V} + 2(p_{\bar{u}} + p_{\bar{d}} + p_{\bar{s}}) = 1,$$

and we finally obtain

$$\begin{aligned} c_G &= A_g\left\{[\gamma_E + \Psi(b_g+2)]^2 - \Psi^{(1)}(b_g+2) + \frac{\pi^2}{6}\right\} \\ &\quad + B_g[\gamma_E + \Psi(b_g+2)] + (b_g+1)[1 - p_{u_V} - dp_V \\ &\quad - 2(p_{\bar{u}} + p_{\bar{d}} + p_{\bar{s}})]. \end{aligned}$$

[1] V. N. Gribov and L. N. Lipatov, Sov. J. Nucl. Phys. **15**, 438 (1972); G. Altarelli and G. Parisi, Nucl. Phys. **B126**, 298 (1977); Yu. L. Dokshitzer, Sov. Phys. JETP **46**, 641 (1977).

[2] G. Curci, W. Furmanski, and R. Petronzio, Nucl. Phys. **B175**, 27 (1980).

[3] W. Furmanski and R. Petronzio, Phys. Lett. **97B**, 437 (1980).

[4] S. Moch, J. A. M. Vermaseren, and A. Vogt, Nucl. Phys. **B688**, 101 (2004).

[5] A. Vogt, S. Moch, and J. A. M. Vermaseren, Nucl. Phys. **B691**, 129 (2004).

[6] A. D. Martin, R. G. Roberts, W. J. Stirling, and R. S. Thorne, Eur. Phys. J. C **23**, 73 (2002).

[7] M. Gluck, E. Reya, and A. Vogt, Eur. Phys. J. C **5**, 461 (1998).

[8] J. Pumplin, D. R. Stump, J. Huston, H. L. Lai, P. Nadolsky, and W. K. Tung, J. High Energy Phys. 07 (2002) 012.

[9] A. M. Cooper-Sarkar, J. Phys. G **28**, 2669 (2002).

[10] S. I. Alekhin, Phys. Rev. D **63**, 094022 (2001).

[11] V. S. Fadin, E. A. Kuraev, and L. N. Lipatov, Phys. Lett. **60B**, 50 (1975); L. N. Lipatov, Yad. Fiz. **23**, 642 (1976) [Sov. J. Nucl. Phys. **23**, 338 (1976)]; I. I. Balitsky and L. N. Lipatov, Yad. Fiz. **28**, 1597 (1978) [Sov. J. Nucl. Phys. **28**, 822 (1978)].

[12] V. S. Fadin and L. N. Lipatov, JETP Lett. **49**, 352 (1989); Yad. Fiz. **50**, 1141 (1989) [Sov. J. Nucl. Phys. A **50**, 712 (1989)].

[13] The reader who wants a modern overview of the S matrix and Regge theory and diffraction can read the books by S. Donnachie, G. Dosch, P. Landshoff, and O. Nachtmann, *Pomeron Physics and QCD* (Cambridge University Press, Cambridge, UK, 2002) and V. Barone and E. Predazzi, *High-Energy Particle Diffraction* (Springer, Berlin, 2002).

[14] T. Regge, Nuovo Cimento **14**, 951 (1959).

[15] T. Regge, Nuovo Cimento **18**, 947 (1960).

[16] K. Hagiwara *et al.*, Phys. Rev. D **66**, 010001 (2002). The data on total cross sections can be obtained from from http://pdg.lbl.gov

[17] A. Donnachie and P. V. Landshoff, Phys. Lett. B **518**, 63 (2001).

[18] J. R. Cudell and G. Soyez, Phys. Lett. B **516**, 77 (2001).

[19] P. Desgrolard and E. Martynov, Eur. Phys. J. C **22**, 479 (2001).

[20] G. Soyez, Phys. Rev. D **67**, 076001 (2003).

[21] L. Csernai, L. Jenkovszky, K. Kontros, A. Lengyel, V. Magas, and F. Paccanoni, Eur. Phys. J. C **24**, 205 (2002).

[22] G. Soyez, Phys. Rev. D **69**, 096005 (2004).

[23] G. Soyez, Phys. Lett. B **603**, 189 (2004).

[24] A. Donnachie and P. V. Landshoff, Phys. Lett. B **533**, 277 (2002).

[25] H1 Collaboration, I. Abt *et al.*, Nucl. Phys. **B407**, 515 (1993).

[26] H1 Collaboration, T. Ahmed *et al.*, Nucl. Phys. **B439**, 471 (1995).

[27] H1 Collaboration, S. Aid *et al.*, Nucl. Phys. **B470**, 3 (1996).

[28] H1 Collaboration, C. Adloff *et al.*, Nucl. Phys. **B497**, 3 (1997).

[29] H1 Collaboration, C. Adloff *et al.*, Eur. Phys. J. C **13**, 609 (2000).

[30] H1 Collaboration, C. Adloff *et al.*, Eur. Phys. J. C **19**, 269 (2001).

[31] H1 Collaboration, C. Adloff *et al.*, Eur. Phys. J. C **21**, 33 (2001).

[32] ZEUS Collaboration, M. Derrick *et al.*, Phys. Lett. B **316**, 412 (1993).

[33] ZEUS Collaboration, M. Derrick *et al.*, Z. Phys. C **65**, 379 (1995).

[34] ZEUS Collaboration, M. Derrick *et al.*, Z. Phys. C **69**, 607 (1996).

[35] ZEUS Collaboration, M. Derrick *et al.*, Z. Phys. C **72**, 399 (1996).

[36] ZEUS Collaboration, J. Breitweg *et al.*, Phys. Lett. B **407**, 432 (1997).

[37] ZEUS Collaboration, J. Breitweg *et al.*, Eur. Phys. J. C **7**, 609 (1999).

[38] ZEUS Collaboration, J. Breitweg *et al.*, Eur. Phys. J. C **12**, 35 (2000).

[39] ZEUS Collaboration, S. Chekanov *et al.*, Eur. Phys. J. C **21**, 443 (2001).

[40] BCDMS Collaboration, A. C. Benvenuti *et al.*, Phys. Lett. B **223**, 485 (1989).

[41] E665 Collaboration, M. R. Adams *et al.*, Phys. Rev. D **54**, 3006 (1996).

[42] New Muon Collaboration, M. Arneodo *et al.*, Nucl. Phys. **B483**, 3 (1997).

[43] L. W. Whitlow, E. M. Riordan, S. Dasu, S. Rock, and A. Bodek, Phys. Lett. B **282**, 475 (1992).

[44] BCDMS Collaboration, A. C. Benvenuti *et al.*, Phys. Lett. B **237**, 595 (1990).

[45] E. Oltman *et al.*, Z. Phys. C **53**, 51 (1992).

[46] W. G. Seligman *et al.*, Phys. Rev. Lett. **79**, 1213 (1997).

[47] CCFR Collaboration, B. T. Fleming *et al.*, Phys. Rev. Lett. **86**, 5430 (2001).

[48] New Muon Collaboration, P. Amaudruz *et al.*, Nucl. Phys. **B371**, 3 (1992).

[49] C. Lopez and F. J. Yndurain, Nucl. Phys. **B171**, 231 (1980).

[50] See e.g. D. W. Sivers, Annu. Rev. Nucl. Part. Sci. **32**, 149 (1982).

[51] S. Dasu *et al.*, Phys. Rev. D **49**, 5641 (1994).

[52] L. L. Jenkovszky, F. Paccanoni, and E. Predazzi, Nucl. Phys. B, Proc. Suppl. **25**, 80 (1992).

[53] P. Desgrolard, M. Giffon, L. L. Enkovsky, A. I. Lengyel, and E. Predazzi, Phys. Lett. B **309**, 191 (1993).

[54] J. R. Cudell, E. Martynov, and G. Soyez, Nucl. Phys. **B682**, 391 (2004).